LANGMUIR

Article

pubs.acs.org/Langmuir

Perfectly Ordered Patterns Formed by a Heterogeneous Nucleation Process of Block Copolymer Self-Assembly Under Rectangular Confinement

Tao Yang,*[,†,‡] Siwen Tian,[†] Yu Zhu,[†] and Weihua Li*[,‡]

[†]Ningxia Key Laboratory of Information Sensing & Intelligent Desert, School of Physics and Electronic-Electrical Engineering, Ningxia University, Yinchuan 750021, China

[‡]State Key Laboratory of Molecular Engineering of Polymers, Department of Macromolecular Science, Fudan University, Shanghai 200433, China

ABSTRACT: The heterogeneous nucleation process during the phase separation of binary blends of the AB diblock and the C homopolymer induced by rectangular confinement is studied by cell dynamics simulation based on the time-dependent Ginzburg−Landau theory. The main goal is to yield large-scale ordered hexagonal patterns by tailoring the surface potentials of the sidewalls. Our study reveals a crucial condition to induce the desired heterogeneous nucleation process in which the nucleated domain grains grow and merge into a defect-free pattern. Specifically, nucleations are induced simultaneously by two parallel sidewalls with a strong surface potential, whereas the spontaneous nucleation and the heterogeneous nucleation at the other two walls with a weak surface potential are suppressed. Moreover, the confinement effect of the other two walls can ensure that the two rows of nucleated domains have correlated positions. Importantly, we find that the ordering process under the crucial condition exhibits a high tolerance to the rectangular sizes. Only a few defects in thousands of domains are occasionally caused that are observed to be annihilated in a short-annealing time via various mechanisms. This study may provide a facile route to prepare large-scale ordered patterns via a simple rectangular confinement.

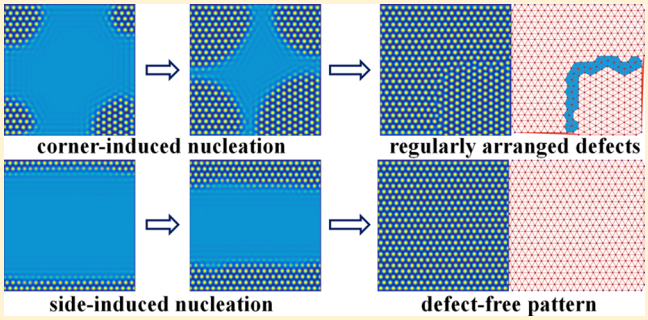

INTRODUCTION

The self-assembly of block copolymers has continuously attracted the interest of scientists from multidisciplinary fields because it leads to the formation of rich ordered nanostructures that exhibit a lot of potential applications in a wide range of fields.[1−5] In particular, as modern synthesis techniques advance, various block copolymers with more complicated architectures and more components can be precisely synthesized in experiments, which opens a huge imaginary space for the fabrication of novel ordered structures.[6] More importantly, recently it has been proposed that block copolymer systems could be devised for the targeting desired interesting structures as long as the valid design principles of molecular architectures are built up according to the established knowledge on the self-assembly mechanisms of known block copolymers. A large number of intriguing structures have been predicted by the self-consistent field theory with the self-assembly of purposely designed block copolymer systems such as linear multiblock terpolymers[7] and binary blends of two distinct block copolymers.[8,9] These advances in both experiment and theory broaden the application perspective of block copolymer self-assembly further.

One of the most promising applications of block copolymers lies in the bottom-up nanolithography technique via the directed self-assembly (DSA) that could lead to large-scale ordered patterns or devise-oriented irregular structures.[4,10−14] These structures can be pattern-transferred into silicon substrates and thus can be used to manufacture high-density storage media[15,16] or structural subunits of integrated circuits.[17,18] Two main directing methods have been well-developed based on chemical (chemoepitaxy)[19−21] and topographical (graphoepitaxy)[22−24] guiding patterns. In graphoepitaxy, the guiding patterns can be specifically designed arrays of nanoposts[18,24,25] or geometrical confinements.[26−28] By contrast, the latter is relatively cheaper to prepare. The directing effect of geometrical confinement is two fold. On the one hand, the presence of geometrical boundaries breaks the space symmetry of the bulk phases of block copolymers and thus results in the formation of novel structures, especially when the geometrical size is small, for example, as large as a few domain spacings.[29−41] On the other hand, the geometrical boundary is able to effectively register the domain positions and guide the orientation of domain array, thus leading to large-scale ordered patterns.[27,28,42,43]

The directing efficiency of DSA is of importance because it dictates the manufacturing cost. For either chemoepitaxy or

Received: October 13, 2016
Revised: November 24, 2016
Published: November 29, 2016

DOI: 10.1021/acs.langmuir.6b03638
Langmuir 2016, 32, 13787−13794

graphoepitaxy, it has been revealed that there exists a bottleneck with the directing efficiency.[44] For example, the direction of a sparse array of nanoposts on the self-assembly of cylinder-forming diblock copolymers could lead to defect-free hexagonal patterns. The experimental work by Bita et al. demonstrates a limit of the directing efficiency that is quantified by density multiplication (DM) defined as the ratio between the self-assembled domain density and that of the prepatterned array of nanoposts, that is, DM < 25.[24] This limit is confirmed by the study of dynamic simulations based on the time-dependent Ginzburg−Landau (TDGL) theory.[44,45] Moreover, the theoretical study reveals that the underlying mechanism for the efficiency limit stems from the phase separation kinetics of block copolymers, that is, the spinodal process or spontaneous nucleation process with an extremely high nucleation rate. Accordingly, a new DSA scheme realized via the heterogeneous nucleation process has been proposed.[46]

The nucleation phenomenon commonly occurs with a first-order phase transition, in which one metastable phase overcomes an energy barrier E_b to transform into a stable phase.[47,48] The nucleation rate p, which quantifies the probability of nucleation events occurring in a unit volume per unit time, is dictated by the magnitude of the energy barrier, that is, $p \propto \exp(-\beta E_b)$, where $\beta = 1/k_B T$ with k_B being the Boltzmann constant and T being the temperature. With a very large p, multiple nucleation events happen simultaneously and densely at random positions in the sample and then grow into domain grains with random orientations. Clusters of defects are avoidably produced on the boundaries between different grains owing to their mismatched positions and orientations, and these clustered defects are usually long-lived relative to experimentally accessible annealing time.[46] Therefore, a low spontaneous nucleation rate is needed for improving the ordering degree of the self-assembled domains by block copolymers. Furthermore, nucleation agents are necessarily introduced to register the nucleation location because a random location of spontaneous nucleation is undesirable in experiments. As a consequence, a set of heterogeneous nucleations at desired positions is induced by purposely designed nucleation agents with a dominantly high nucleation rate over the spontaneous ones, and their grown domain grains with a consistent orientation and commensurate positions merge into a single-crystal pattern.

On the basis of the above arguments, two types of nucleation agents have been devised to illustrate the validity of the DSA scheme of heterogeneous nucleation in a cylinder-forming block copolymer system that is composed of an AB diblock copolymer and a C homopolymer.[46,49] The concentration of the C homopolymer instead of the temperature is successfully used to regulate the spontaneous nucleation rate from high to low. One type is the sparse periodic array of anisotropic potential fields (e.g., a pair of potential wells), which is capable of yielding a much higher DM than the limit of DM = 25 for the perfect hexagonal pattern.[46] An obvious weakness in the preparation of the agent unit is its feature size being as small as the block copolymer domain. The other type of nucleation agent is acted by the lateral hexagonal confinement, in which six corners give rise to a higher nucleation rate than the spontaneous one as well as the side-induced one.[49] Six corner-induced domain grains whose locations are commensurate with the domain spacing grow and finally merge into a perfectly ordered hexagonal pattern under the direction of six sidewalls. Importantly, the heterogeneous nucleation phenomenon in the block copolymer system has been rationalized by the classical nucleation theory.

In the DSA scheme of the hexagonal confinement, the preparation of the hexagonal well is critical. Although there is no technical difficulty with modern lithography techniques, it should be technically easier to prepare a rectangular well than a hexagonal one. In other words, it will make the DSA scheme more facile by replacing the hexagonal confinement with a rectangular one. However, the rectangular coordinate is apparently incommensurate with the crystal lattice of hexagonal cylinders.[26,42] To validate the DSA scheme of heterogeneous nucleation in a rectangular confinement presents an interesting challenge.

A possible strategy is to alter the surface potentials of sidewalls to be unequal, that is, that the two sidewalls along one direction have an equal surface potential but differing from that of the other sidewalls. Without loss of generality, we assume that the two walls along the x direction have a stronger surface potential than the other two walls along the y direction. Accordingly, the two walls along the x direction act as the major nucleation agent with a higher nucleation rate than that of the other two walls. In other words, two lines of nucleations are simultaneously induced at the two walls along the x direction and then grow to meet with each other. Additionally, the position correlation between the two rows of domains can be regulated by the confining effect of the other two walls with a neutral surface or weak surface potential at the y direction. In this study, our main goal is to achieve the DSA strategy based on the heterogeneous nucleation that occurred within the microphase separation of the AB/C binary blends under the rectangular confinement by tailoring the surface potentials of the four sidewalls. Similar to our previous study,[46,49] the phase separation dynamics is examined by the TDGL simulations.

MODEL AND THEORY

We consider a binary blend composed of an AB diblock copolymer and a C homopolymer (AB/C) laterally confined in a rectangular well with sizes of L_x and L_y at the x and y directions, respectively. The micro-/macrophase separation of the three-component system can be phenomenologically described by a developed Ginzburg−Landau mean-field theory by Ohta and Ito[50] based on the Ohta−Kawasaki model for the microphase separation of the AB diblock copolymer.[51] In this model, many parameters such as the chain lengths and interaction parameters are not explicitly included, and instead they are replaced by a set of phenomenological parameters. With regard to the physical meanings of these parameters, we refer readers to the original literature[50] or to our previous work,[46,49] and thus we do not repeat the explanations here. We would like to emphasize that this AB/C binary model is intentionally developed to model the AB/B blend by tailoring the related interaction parameters.[46,52] Specifically, the stability of the disordered state relative to the considered ordered phase is controlled by the addition of homopolymers from stable to metastable and unstable. In fact, the main aim of utilizing the C homopolymer instead of the B homopolymer is to overcome the modeling difficulty in the Ginzburg−Landau mean-field theory for the AB/B blend.[50]

Two characteristic parameters for this AB/C blend are the concentration of C homopolymer $\bar{\phi}_C$ and the block ratio of the A block f in the AB diblock copolymer. We choose two independent order parameters to describe the phase separation of the three-component system, $\phi(\mathbf{r}) = \phi_A(\mathbf{r}) - \phi_B(\mathbf{r})$ and $\eta(\mathbf{r})$

DOI: 10.1021/acs.langmuir.6b03638
Langmuir 2016, 32, 13787−13794

$= \phi_A(\mathbf{r}) + \phi_B(\mathbf{r}) - \Psi_C$, where $\phi_K(\mathbf{r})$ (K = A, B, and C) denotes the local density of the K component at a given position $\mathbf{r}$, and Ψ_C is a constant used to regulate the occurrence of possible macrophase separation. Then the free energy can be expressed as a functional of the two spatial functions, $\phi(\mathbf{r})$ and $\eta(\mathbf{r})$

$$F[\phi, \eta] = F_S[\phi, \eta] + F_L[\phi, \eta] + \int d\mathbf{r}\, H_{ext}(\mathbf{r})\phi(\mathbf{r}) \quad (1)$$

where F_S is the short-range contribution originating from the standard Ginzburg−Landau free energy and is composed of interfacial energy and local interaction energy

$$F_S[\phi, \eta] = \int d\mathbf{r}\left\{\frac{D_1}{2}[\nabla\phi(\mathbf{r})]^2 + \frac{D_2}{2}[\nabla\eta(\mathbf{r})]^2 + f_\phi[\phi] + f_\eta[\eta] + f_{int}[\phi, \eta]\right\} \quad (2)$$

Here, D_1 and D_2 are the two positive constants related to the interfacial tensions between the three immiscible components. The local energy terms $f_\phi[\phi]$ and $f_\eta[\eta]$ can be conveniently given by their derivatives $df_\phi/d\phi = -A_\phi \tanh \phi + \phi$ and $df_\eta/d\eta = -A_\eta \tanh \eta + \eta$ with the two parameters $A_\phi > 1$ and $A_\eta > 1$. The last term $f_{int}[\phi, \eta]$ includes a number of intercrossing terms of ϕ and η supplementing the interactions between the three components, $f_{int} = b_1\eta\phi - b_2\eta\phi^2/2 - b_3(\eta\phi^3 + \eta^2\phi + \eta^3\phi) + b_4\eta^2\phi^2/2$. The coefficients of b_1, b_2, b_3, and b_4 have explicit physical meanings qualitatively related to the properties of the AB/C blend.

Similar to the Ohta−Kawasaki free energy,[51] the long-range term, F_L, is specifically constructed as

$$F_L[\phi, \eta] = \int d\mathbf{r}\int d\mathbf{r}' G(\mathbf{r}, \mathbf{r}')\left[\frac{\alpha}{2}\delta\phi(\mathbf{r})\delta\phi(\mathbf{r}') + \beta\delta\phi(\mathbf{r})\delta\eta(\mathbf{r}') + \frac{\gamma}{2}\delta\eta(\mathbf{r})\delta\eta(\mathbf{r}')\right] \quad (3)$$

where $\delta\phi(\mathbf{r}) = \phi(\mathbf{r}) - \bar{\phi}$, $\delta\eta(\mathbf{r}) = \eta(\mathbf{r}) - \bar{\eta}$. $\bar{\phi}$ and $\bar{\eta}$ indicate the spatial average of $\phi(\mathbf{r})$ and $\eta(\mathbf{r})$, respectively. The coefficients α, β, and γ satisfy the relation of $\beta^2 = \alpha\gamma$ and they are related to the polymerization degrees of AB and C.[50] In eq 3, the Green function $G(\mathbf{r}, \mathbf{r}')$ takes the Coulomb interaction form characterizing the long-range feature of the chain connectivity of the diblock copolymer.

In eq 1, the last term gives the interaction energy of the polymers with the wall surfaces of the rectangular well, and the spatial function $H_{ext}(\mathbf{r})$ is introduced to model the surface potentials of the four walls. A similar expression of $H_{ext}(\mathbf{r})$ as in our previous study is used[49]

$$H_{ext}(\mathbf{r}) = \frac{1}{2}\Lambda_i\{\tanh[(\sigma - d(\mathbf{r}))/\varepsilon] + 1\} \quad (4)$$

where the shortest distance of the position $\mathbf{r}$ to the four walls is $d(\mathbf{r}) < 2\sigma$. Λ_i, 2σ, and ε denote the field strength of the walls at the i direction ($i = x, y$), interaction range, and potential steepness, respectively. With the free energy functional in eq 1, the phase separation dynamics of the AB/C blend is described by the two conserved Cahn−Hilliard dynamic equations

$$\frac{\partial\phi}{\partial t} = M_1\nabla^2\frac{\delta F[\phi, \eta]}{\delta\phi} + \xi_\phi(\mathbf{r}, t)$$
$$\frac{\partial\eta}{\partial t} = M_2\nabla^2\frac{\delta F[\phi, \eta]}{\delta\eta} + \xi_\eta(\mathbf{r}, t) \quad (5)$$

where M_1 and M_2 are the two mobility coefficients, and ξ_ϕ and ξ_η are the random noise terms that satisfy the fluctuation dissipation theorem. Similar to our previous work, we specify the blending system by choosing $f = 0.40$, $D_1 = 0.5$, $D_2 = 1.0$, $M_1 = M_2 = 1.0$, $A_\phi = 1.26$, $A_\eta = 1.10$, $b_1 = -0.05$, $b_2 = 0.05$, $b_3 = 0.01$, $b_4 = 0.10$, $\Psi_C = 0.20$, $\sigma = 0.15L_0$, and $\varepsilon = 0.5L_0$, where L_0 indicates the cylinder-to-cylinder distance and varies as $\bar{\phi}_C$. Note that a negative value of b_1 is required to properly describe the miscibility between the AB diblock and the C-mimicking B homopolymer that could lead to microphase or macrophase separation. To simulate the systems as large as microns, the dynamic equations are integrated in the two-dimensional space by cell dynamics simulation (CDS) with the spatial discretization $\Delta x = \Delta y = 0.5$ and the time step $\Delta t = 0.1$.

RESULTS AND DISCUSSION

It has been known that the current AB/C blend with $\bar{\phi}_C < 0.10$ forms the hexagonal phase in the two-dimensional space,[46] and its phase separation kinetics is effectively regulated by $\bar{\phi}_C$ from multiple nucleations (e.g., spinodal) with a very high nucleation rate and a negligibly short incubation time at $\bar{\phi}_C = 0.10$ to the rare nucleation with a considerably low nucleation rate accompanied by a prolonged incubation process at $\bar{\phi}_C < 0.04$. The nucleation process with a low spontaneous nucleation rate satisfies the requirement by the DSA scheme of heterogeneous nucleation to let the spontaneous nucleation make a concession to the heterogeneous nucleation induced by external nucleation agents. In this study, we simply fix $\bar{\phi}_C = 0.025$ to maintain the low spontaneous nucleation rate, of which the cylinder-to-cylinder distance is estimated to be $L_0 \approx 18.8\Delta x$ in our simulations. On the other hand, our previous work indicates that the heterogeneous nucleation rate can be readily tuned by the strength of the surface potentials of the confining walls. Here, we will systematically study the influence of the two strengths Λ_x and Λ_y on the heterogeneous nucleation process and thus on the ordering process of the hexagonal pattern in the entire rectangular sample. Specifically, we focus on the case where all sidewalls attract the majority component, that is, $\Lambda_x > 0$ and $\Lambda_y > 0$.

To exclusively illuminate the influence of the coordinate angle of 90° that is mismatched with the hexagonal lattice of the block copolymer domains, in contrast to the commensurate angle of 120° of the hexagonal confinement, we first consider the square-well confinement with an equal field strength $\Lambda_x = \Lambda_y = \Lambda$. The size of the square well is chosen as large as $L_x = L_y = 60L_0$ that is around 2 μm for diblock copolymers with a moderate molecular weight. Typical morphological snapshots at three different time steps for various field strengths are presented in Figure 1. To visualize the ordering degree of the morphologies formed at the critical time t_c when the phase separation just expands to fill the entire sample, their corresponding Delaunay triangular plots are shown in the bottom row. At the left column, $\Lambda = 0.002$ produces a rather weak surface preference leading to the corner-induced nucleations but not to the side-induced nucleations.[49] Surprisingly, all four nucleation domain grains are single crystalline and are oriented with their (10) crystal face aligning along one of the sidewalls. This specific orientation ingeniously circumvents the angle mismatch of the square well and the hexagonal lattice. However, the alignment of the (10) face is randomly selected to be along the x or y direction. For instance, in Figure 1a1, the (10) face of the bottom-left grain is along the x direction, whereas the others are along the y direction.

DOI: 10.1021/acs.langmuir.6b03638
Langmuir 2016, 32, 13787−13794

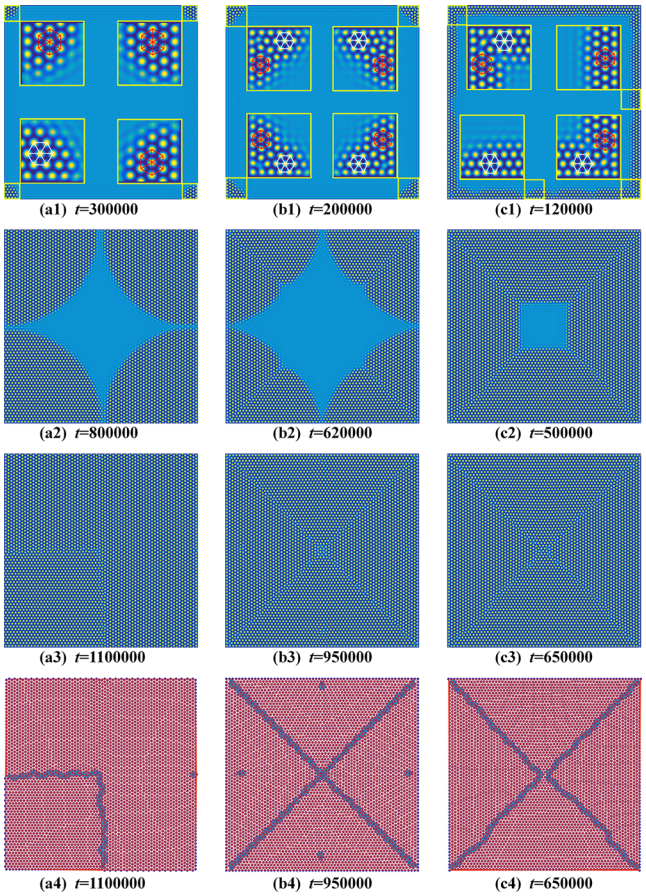

Figure 1. Morphological snapshots at three different time steps within the heterogeneous nucleation processes of the AB/C blends occurred under the induction of a square well with a fixed size of $L_x = L_y = 60L_0$ and various field strengths: (a) $\Lambda = 0.002$ (left column), (b) $\Lambda = 0.003$ (middle column), and (c) $\Lambda = 0.007$ (right column). Positive field strength indicates a surface preference to the majority component. The Delaunay triangles for the third-row morphologies formed at the critical time t_c when the domain grains grow up to fill the entire square well are plotted in the bottom row, highlighting the defective areas. The number of defects and total domains in (a4−c4) is (n_{DF}, n_{domain}) = (61, 4247), (176, 4242), and (156, 4290), respectively. Insets of the three snapshots in the top row enlarge the areas at four corners, where the orientation of each domain grain is indicated by a hexagonal unit in white for the (10) crystal face aligned along the x direction and in red for the (10) crystal face aligned along the y direction.

Although each grown domain grain is perfectly ordered, the inconsistent alignment causes additional defects onto their boundaries besides those induced by the possibly uncorrelated positions. As a result, a large cluster of defects is observed as shown in Figure 1a4.

Another corner-induced nucleation process is demonstrated with $\Lambda = 0.003$ in Figure 1b. In contrast to the sample of $\Lambda = 0.002$ in Figure 1a, the corner-induced nucleations are remarkably different, with respect to the alignment of the domain crystal. Obviously, each nucleation results in twin crystalline grains of which the (10) faces are separately aligned along the x and y directions. As a consequence, a line of clustered defects occurs along the diagonal delimiting the two grains at each corner, and finally these defects at the four corners constitute two diagonal lines of defects crossing over the entire square sample. This corner-induced twin-grain nucleation process provides a strategy to generate regularly arranged defects that might have specific applications in the field of photonic crystals.[53,54]

As the field strength Λ increases further, the side-induced nucleation rate becomes considerably high and thus each sidewall starts to act as the effective nucleation agent. In Figure 1c with $\Lambda = 0.007$, nuclei are induced simultaneously at the four walls after a short incubation time relative to that of $\Lambda = 0.002$ or 0.003. Then, these nucleated domain grains grow synchronously forming a nearly flat front surface along each side. In other words, the square disordered region is maintained, and it consistently shrinks with time until the phase separation expands the entire sample. Interestingly, similar to the case of corner-induced nucleation at $\Lambda = 0.003$, two diagonal lines of defects are caused by the merging of distinct nucleation grains at two orthogonal sidewalls. From Delaunay triangles, the number of defects mainly composed of five- and seven-fold dislocations, n_{DF}, can be readily accounted, and thus the defect concentration defined as $f_{DF} = n_{DF}/n_{domain} \times 100\%$ is estimated, where n_{domain} indicates the total number of domains contained in the sample. As the defect concentration fluctuates with the sample, the average concentration $\langle f_{DF} \rangle$ is calculated by averaging eight independent runs of each sample. For example, (n_{DF}, n_{domain}) = (61, 4247), (176, 4242), and (156, 4290) for Figure 1a4−c4, and their average concentration of defects are $\langle f_{DF} \rangle$ = (1.54 ± 0.47)%, (4.16 ± 0.12)%, and (3.84 ± 0.12)%, respectively. Note that the larger fluctuation of $\langle f_{DF} \rangle$ in Figure 1a than the other two cases originates from the random selection for the alignment of the (10) crystal face of the domain grain nucleated at each corner.

The above-mentioned simulations elucidate the intrinsic difficulty of yielding defect-free hexagonal patterns with the DSA scheme of heterogeneous nucleation induced by a square/rectangular confinement. However, the sample at $\Lambda = 0.002$ generates a hexagonal pattern with a low concentration of defects 1.54%, which are mainly the result of the merging of nucleation grains with orthogonal orientations. This is instructive for us to achieve a perfect pattern by orientating all nucleated domain grains along a single direction. Additionally, the two samples in Figure 1b,c with rather strong surface potentials suggest that the strong surface preference can register the alignment of the (10) crystal face along the induction sidewall. Accordingly, a simple route can be speculated that two pairs of sidewalls are set to have unequal surface preferences. The surface potential of one pair of sidewalls, for example, at the x direction, is selected to be so strong that it can induce nucleations along the entire side, that is, $\Lambda_x \geq 0.004$, whereas the surface potential of the other two sidewalls at the y direction must be set to be weak, that is, $\Lambda_y \geq 0.003$, which would not induce any nucleation at the sidewalls to intervene in the growth of the domain grains induced by the x sidewalls. Therefore, in the following paragraphs, we will focus on the heterogeneous nucleation process occurring in the rectangular well with $\Lambda_x > \Lambda_y$ and $L_x \neq L_y$, aiming to obtain a parameter window of the two field strengths for the self-assembly of the perfect hexagonal pattern. To make the rectangular sizes be commensurate with the hexagonal lattice of domains, we intentionally choose $L_x = m_x L_0$ and $L_y = (m_y + 0.5)\sqrt{3}L_0$, respectively, where m_x and m_y are the two integer numbers, for example, $m_x = 60$ and $m_y = 30$.

To elucidate the effect of Λ_y on the ordering process, we present the morphological snapshots of heterogeneous

DOI: 10.1021/acs.langmuir.6b03638
Langmuir 2016, 32, 13787−13794

nucleation for fixed Λ_x = 0.007 and three distinct values of (a) Λ_y = 0.004, (b) 0.0035, and (c) 0.0030 in Figure 2. Similar to

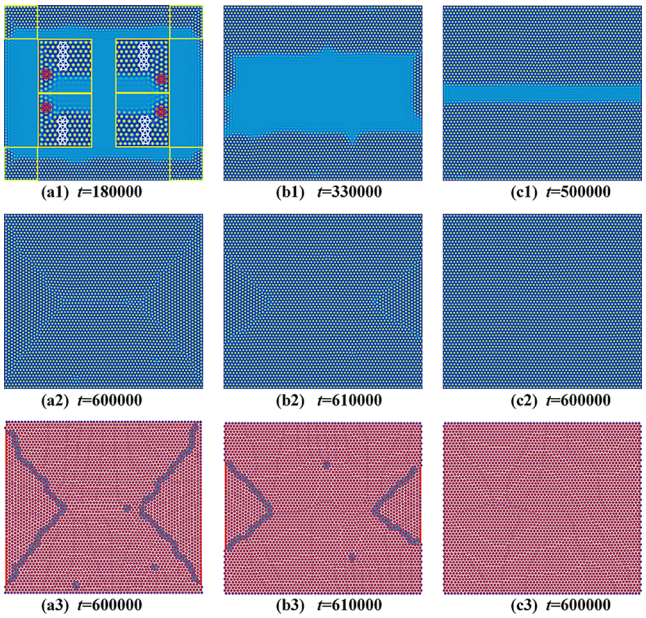

Figure 2. Morphological snapshots and the correspondent Delaunay triangular plots for the morphologies at the critical time $t = t_c$ formed by the heterogeneous nucleation process induced by the rectangular confinement with sizes $L_x \times L_y = 60\ L_0 \times 30.5\sqrt{3}\ L_0$ and fixed field strength Λ_x = 0.007. (a–c) Correspond to three different values of Λ_y = 0.004, 0.0035, and 0.003, respectively. In (a–c), the number of defects and domains is (n_{DF}, n_{domain}) = (126, 3790), (76, 3807), and (0, 3812), respectively.

Figure 1c, the field strength of Λ_x = 0.007 is strong enough for side-induced nucleations at the x sidewalls. As expected, side-induced nucleations occur at the x sidewalls in all three cases. However, in Figure 2a,b, other nucleation events also occur simultaneously or during the growth period of the side-induced domain grains at the x direction. For instance, in Figure 2a, twin crystalline grains are induced at each corner similar to Figure 1b because two joined sidewalls have a competitive induction ability of nucleation, leading to four lines of clustered defects. The condition of $\Lambda_x > \Lambda_y$ tilts the lines toward the y sidewalls. As Λ_y is decreased to 0.0035 in Figure 2b, the side-induced nucleations at the x sidewalls dominate those at the y sidewalls, and thus a single crystalline grain is yielded at each x sidewall. Nevertheless, the perfectly ordered pattern is not achieved because of another reason; that side-induced nucleations at the y sidewalls occur during the growth period of the domain grains at the x sidewalls. The two groups of domain grains have orthogonal (10) crystal faces, and thereby their final fusion results in the formation of clustered defects on their boundaries. Compared with the sample in Figure 2a with $\langle f_{DF} \rangle$ = (3.64 ± 0.19)%, the defect lines are shortened by the shrunken domain grains at the y sidewalls, leading to a lower defect concentration $\langle f_{DF} \rangle$ = (2.28 ± 0.21)%. When Λ_y is lowered to 0.003 in Figure 2c, two rows of domains are exclusively nucleated at the two x sidewalls, and the two domain grains synchronically grow forming a nearly flat advancing front until they merge into a single crystalline grain. This sample demonstrates an ideal heterogeneous nucleation process for the DSA scheme by the rectangular confinement, leading to the desired ordered pattern.

To show the effect of Λ_y on the directing effect at a more quantitative manner, we present the average defect concentration $\langle f_{DF} \rangle$ of the morphologies at the critical time t_c as a function of Λ_y for three given magnitudes of Λ_x = 0.004, 0.010, and 0.015 in Figure 3. Note that Λ_x = 0.015 corresponds to a

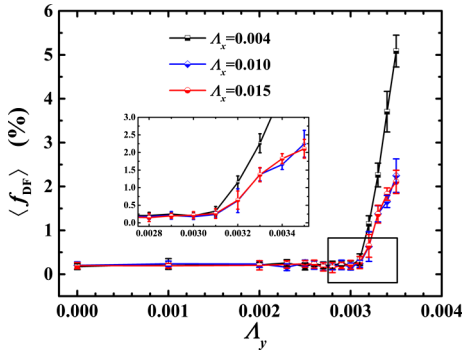

Figure 3. Average defect concentration $\langle f_{DF} \rangle$ of the morphologies at t_c as a function of Λ_y for three given values of Λ_x = 0.004, 0.010, and 0.150. The inset enlarges the portion around the critical value of Λ_y where $\langle f_{DF} \rangle$ increases abruptly. The errors are estimated by averaging eight independent runs of each sample.

rather strong field strength.[49] In fact, a field strength of Λ_x > 0.015 can cause a notable compaction of the domains near the wall surface at the normal direction, even leading to a fusion of domains in the first layer of minority domains at the x sidewalls. Interestingly, there exists a critical magnitude of $\Lambda_y^* \approx 0.003$ at which $\langle f_{DF} \rangle$ undergoes an abrupt change. For $\Lambda_y < \Lambda_y^*$, the defect concentration at $t = t_c$ is maintained at an extremely low level, that is, $\langle f_{DF} \rangle \approx 0.2\%$. The defects at this concentration level usually exist as isolated five-seven dislocation pairs and can be thermally annealed out in an extra time after $t = t_c$. When $\Lambda_y > \Lambda_y^*$, $\langle f_{DF} \rangle$ abruptly increases because of the generating mechanism of defects elucidated in the previous paragraph. In a word, to ensure the directing effect of the DSA scheme based on the heterogeneous nucleation under the induction of the rectangular confinement, the surface field at the y sidewalls has to be kept to be weaker than a critical value, that is, $\Lambda_y < \Lambda_y^*$, whereas the field strength at the x sidewalls exhibits a very wide window of $0.004 \lesssim \Lambda_x \lesssim 0.015$.

In topographical DSA schemes, the tolerance of the directing effect to the geometrical sizes is of importance because it dictates their feasibility from a practical point of view. The previous results reveal a limited tolerance window to the hexagonal size relative to the domain spacing for the DSA scheme of hexagonal confinement.[49] To examine the size tolerance of the current DSA scheme, we estimate the defect concentration $\langle f_{DF} \rangle$ as a function of L_x for fixed $L_y = 30.5\sqrt{3}\ L_0$ (a) and that as a function of L_y for fixed $L_x = 60 L_0$ (b) in Figure 4. The field strengths are chosen as Λ_x = 0.007 and Λ_y = 0.0015. Although $\langle f_{DF} \rangle$ fluctuates as L_x or L_y varies, it does not exhibit a sensitive correlation with the sizes, and instead it exhibits a stochastic behavior. More importantly, the defect concentration with a small fluctuation amplitude is kept within a very narrow range of $0 \lesssim \langle f_{DF} \rangle \lesssim 0.4\%$. This implies that the directing effect is hardly dependent on the rectangular size. In other words, this DSA scheme does not exhibit an obvious limit with the directing efficiency in theory.

DOI: 10.1021/acs.langmuir.6b03638
Langmuir 2016, 32, 13787–13794

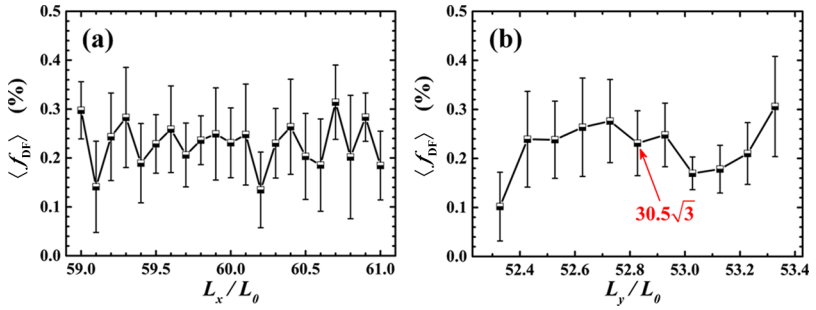

Figure 4. Defect concentration $\langle f_{DF} \rangle$ as a function of L_x for fixed $L_y = 30.5\sqrt{3}\ L_0$ (a) and that as a function of L_y for fixed $L_x = 60L_0$ (b).

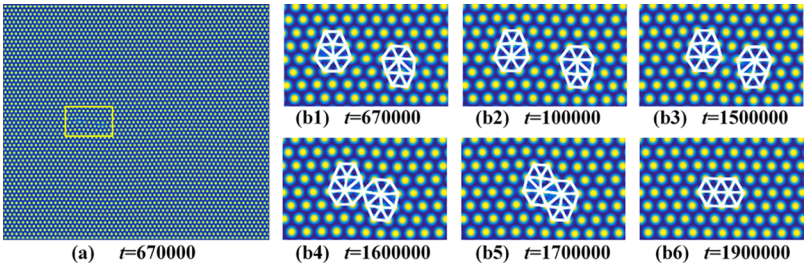

Figure 5. (b1−b6) Snapshots of two pairs of five-seven dislocations with nearly opposite Burgers vectors observed during the annealing process of the morphology of (a) formed in the rectangular well with $\langle L_x, L_y \rangle = (60L_0, 30.5\sqrt{3}L_0)$ and $(\Lambda_x, \Lambda_y) = (0.0150, 0.0028)$, which move toward each other with time and finally cancel each other.

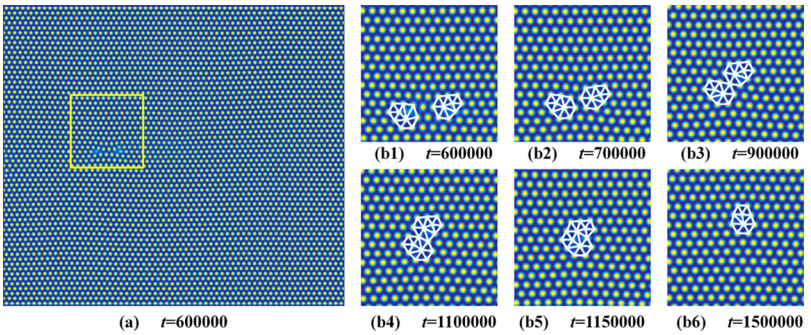

Figure 6. (b1−b6) Snapshots of two pairs of five-seven dislocations with approximately perpendicular Burgers vectors from the morphology of (a) formed in the similar system as that in Figure 5 that collide into a new pair of five-seven dislocations after approaching each other.

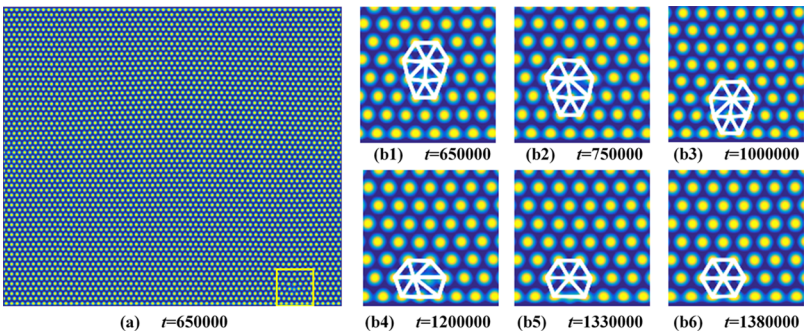

Figure 7. (b1−b6) Snapshots of a single pair of five-seven dislocations observed in the morphology of (a) under the rectangular confinement with $(L_x, L_y) = (60L_0, 30.5\sqrt{3}L_0)$ and $(\Lambda_x, \Lambda_y) = (0.0150, 0.0027)$ that travels to arrive at the bottom x sidewall and then is annihilated.

In addition to the directing effect, the ordering process of the defective morphologies after the critical time is of interest because it proceeds via defect annihilation. Similar to hard condensed matter systems, defects and their stability or annihilation mechanism in the self-assembly of block copolymers represent a kind of very attractive problem because of not only their possible potential applications but also the involved unique processes, for example, deformation, creation, and destruction of the soft domains.[14] During our dynamic simulations, various annihilation mechanisms of defects are observed. In Figure 5, two pairs of five-seven dislocations with nearly opposite Burgers vectors are observed in one of the

DOI: 10.1021/acs.langmuir.6b03638
Langmuir 2016, 32, 13787−13794

morphologies with (Λ_x, Λ_y) = (0.0150, 0.0028). As the annealing process proceeds in the post-growth period, the two pairs of defects move toward each other under a long-range strain-mediated attractive interaction until they collide together.[14] Owing to the opposite Burgers vectors, the collision leads to the annihilation of the two pairs of defects.[14] By contrast, the other two pairs of defects with Burgers vectors forming an angle of 120° in Figure 6 do not cancel each other by collision, and instead they evolve into a new pair of five-seven dislocations. Besides the two collision mechanisms of dislocation pairs, the annihilation process of a single pair of five-seven dislocations is also observed in Figure 7. Typically, a single pair of defects prefers to move toward one x sidewall and then is removed at the boundary.

CONCLUSIONS

In summary, the phase separation kinetics of binary blends of the AB diblock copolymer and the C homopolymer is systematically simulated using the CDS based on the TDGL, demonstrating a heterogeneous nucleation process occurred under the direction of a rectangular confinement that leads to the perfectly ordered hexagonal pattern. To make a comparison with the AB/C blending system confined in a hexagonal well, we first examine the occurrence of heterogeneous nucleation in a square well with a uniform surface potential. Three typical cases of nucleations are observed with various field strengths, including the two types of corner-induced nucleations and one type of side-induced nucleations. In these cases, the defects are unavoidably generated on the boundaries of domain grains with dissimilar orientations. This implies an intrinsic difficulty of yielding the perfect hexagonal patterns with the rectangular confinement whose sidewalls have a uniform surface potential.

Then we turn to the case in which one pair of parallel sidewalls, for example, at the x direction, has a stronger surface potential than the other. In this case, the two sidewalls at the x direction result in lines of nucleation domains at their surfaces, whereas the others at the y direction ensure that the domain grains possess correlated positions at the x direction. Our simulations predict a parameter window of the field strengths Λ_x and Λ_y for the effective direction toward the perfect pattern, in which the field strength Λ_x must be larger than a critical value and can be varied within a wide range, whereas Λ_y must be smaller than a low critical value. Importantly, the DSA scheme based on the heterogeneous nucleation that occurred in the rectangular well with tailored surface potentials exhibits a strong tolerance to the rectangular sizes. Only a few defects in thousands of domains are occasionally caused that are observed to be annihilated in a reasonable annealing time via various mechanisms. Two colliding mechanisms between two pairs of five-seven dislocations are observed. One mechanism is that two pairs of dislocations with nearly opposite Burgers vectors cancel each other after collision.[14] In the other mechanism, two pairs of dislocations with Burgers vectors forming an angle of 120° collide into a new pair of dislocations that can survive during a rather long annealing time. Usually, a single pair of dislocations is removed until it reaches one of the sidewalls. In brief, this study may provide a facile route to prepare large-scale ordered patterns via a simple rectangular confinement.

AUTHOR INFORMATION

Corresponding Authors

*E-mail: yang_tao@alumni.sjtu.edu.cn. Phone: +86 (0)951 2061004. Fax: +86 (0)951 2061004 (T.Y.).

*E-mail: weihuali@fudan.edu.cn. Phone: +86 (0)21 65643579. Fax: +86 (0)21 65640293 (W.L.).

ORCID

Weihua Li: 0000-0002-5133-0267

Notes

The authors declare no competing financial interest.

ACKNOWLEDGMENTS

T.Y. thanks the fundings support by the Natural Science Foundation of Ningxia (Grant no. NZ1640) and National Natural Science Foundation of China (NSFC) (Grant no. 11504190). W.H.L. acknowledges the funding support by NSFC (Grant nos. 21322407 and 21574026).

REFERENCES

(1) Bates, F. S.; Fredrickson, G. H. Block Copolymer Thermodynamics: Theory and Experiment. *Annu. Rev. Phys. Chem.* **1990**, *41*, 525−557.

(2) Park, C.; Yoon, J.; Thomas, E. L. Enabling Nanotechnology with Self Assembled Block Copolymer Patterns. *Polymer* **2003**, *44*, 6725−6760.

(3) Hamley, I. W. Ordering in Thin Films of Block Copolymers: Fundamentals to Potential Applications. *Prog. Polym. Sci.* **2009**, *34*, 1161−1210.

(4) Kim, H.-C.; Park, S.-M.; Hinsberg, W. D. Block Copolymer Based Nanostructures: Materials, Processes, and Applications to Electronics. *Chem. Rev.* **2010**, *110*, 146−177.

(5) Li, W.; Müller, M. Directed Self-Assembly of Block Copolymers by Chemical or Topographical Guiding Patterns: Optimizing Molecular Architecture, Thin-Film Properties, and Kinetics. *Prog. Polym. Sci.* **2016**, *54*−*55*, 47−75.

(6) Bates, F. S.; Hillmyer, M. A.; Lodge, T. P.; Bates, C. M.; Delaney, K. T.; Fredrickson, G. H. Multiblock Polymers: Panacea or Pandora's Box? *Science* **2012**, *336*, 434−440.

(7) Xie, N.; Liu, M.; Deng, H.; Li, W.; Qiu, F.; Shi, A.-C. Macromolecular Metallurgy of Binary Mesocrystals via Designed Multiblock Terpolymers. *J. Am. Chem. Soc.* **2014**, *136*, 2974−2977.

(8) Liu, M.; Xia, B.; Li, W.; Qiu, F.; Shi, A.-C. Self-Assembly of Binary Mesocrystals from Blends of BABCB Multiblock Copolymers and ABC Triblock Copolymers. *Macromolecules* **2015**, *48*, 3386−3394.

(9) Liu, M.; Qiang, Y.; Li, W.; Qiu, F.; Shi, A.-C. Stabilizing the Frank-Kasper Phases via Binary Blends of AB Diblock Copolymers. *ACS Macro Lett.* **2016**, *5*, 1167−1171.

(10) Segalman, R. A. Patterning with Block Copolymer Thin Films. *Mater. Sci. Eng., R* **2005**, *48*, 191−226.

(11) Herr, D. J. C. Directed Block Copolymer Self-Assembly for Nanoelectronics Fabrication. *J. Mater. Res.* **2011**, *26*, 122−139.

(12) Koo, K.; Ahn, H.; Kim, S.-W.; Ryu, D. Y.; Russell, T. P. Directed Self-Assembly of Block Copolymers in the Extreme: Guiding Microdomains from the Small to the Large. *Soft Matter* **2013**, *9*, 9059−9071.

(13) Luo, M.; Epps, T. H. Directed Block Copolymer Thin Film Self-Assembled: Emerging Trends in Nanopattern Fabrication. *Macromolecules* **2013**, *46*, 7567−7579.

(14) Li, W.; Müller, M. Defects in the Self-Assembly of Block Copolymers and Their Relevance for Directed Self-Assembly. *Annu. Rev. Chem. Biomol. Eng.* **2015**, *6*, 187−216.

(15) Park, M.; Harrison, C.; Chaikin, P. M.; Register, R. A.; Adamson, D. H. Block Copolymer Lithography: Periodic Arrays of ~10^{11} Holes in 1 Square Centimeter. *Science* **1997**, *276*, 1401−1404.

(16) Cheng, J. Y.; Ross, C. A.; Thomas, E. L.; Smith, H. I.; Vancso, G. J. Fabrication of Nanostructures with Long-Range Order Using Block Copolymer Lithography. *Appl. Phys. Lett.* **2002**, *81*, 3657−3659.

(17) Stoykovich, M. P.; Müller, M.; Kim, S. O.; Solak, H. H.; Edwards, E. W.; de Pablo, J. J.; Nealey, P. F. Directed Assembly of Block Copolymer Blends into Nonregular Device-Oriented Structures. *Science* **2005**, *308*, 1442−1446.

DOI: 10.1021/acs.langmuir.6b03638
Langmuir 2016, 32, 13787−13794

(18) Chang, J.-B.; Choi, H. K.; Hannon, A. F.; Alexander-Katz, A.; Ross, C. A.; Berggren, K. K. Design Rules for Self-Assembled Block Copolymer Patterns Using Tiled Templates. *Nat. Commun.* **2014**, *5*, 3305.
(19) Kim, S. O.; Solak, H. H.; Stoykovich, M. P.; Ferrier, N. J.; de Pablo, J. J.; Nealey, P. F. Epitaxial Self-Assembly of Block Copolymers On Lithographically Defined Nanopatterned Substrates. *Nature* **2003**, *424*, 411−414.
(20) Ruiz, R.; Kang, H.; Detcheverry, F. A.; Dobisz, E.; Kercher, D. S.; Albrecht, T. R.; de Pablo, J. J.; Nealey, P. F. Density Multiplication and Improved Lithography by Directed Block Copolymer Assembly. *Science* **2008**, *321*, 936−939.
(21) Wan, L.; Yang, X. Directed Self-Assembly of Cylinder-Forming Block Copolymers: Prepatterning Effect on Pattern Quality and Density Multiplication Factor. *Langmuir* **2009**, *25*, 12408−12413.
(22) Segalman, R. A.; Yokoyama, H.; Kramer, E. J. Graphoepitaxy of Spherical Domain Block Copolymer Films. *Adv. Mater.* **2001**, *13*, 1152−1155.
(23) Cheng, J. Y.; Mayes, A. M.; Ross, C. A. Nanostructure Engineering by Templated Self-Assembly of Block Copolymers. *Nat. Mater.* **2004**, *3*, 823−828.
(24) Bita, I.; Yang, J. K. W.; Jung, Y. S.; Ross, C. A.; Thomas, E. L.; Berggren, K. K. Graphoepitaxy of Self-Assembled Block Copolymers on Two-Dimensional Periodic Patterned Templates. *Science* **2008**, *321*, 939−943.
(25) Zhang, L.; Wang, L.; Lin, J. Harnessing Anisotropic Nanoposts to Enhance Long-Range Orientation Order of Directed Self-Assembly Nanostructures via Large Cell Simulations. *ACS Macro Lett.* **2014**, *3*, 712−716.
(26) Hur, S.-M.; García-Cervera, C. J.; Kramer, E. J.; Fredrickson, G. H. SCFT Simulations of Thin Film Blends of Block Copolymer and Homopolymer Laterally Confined in a Square Well. *Macromolecules* **2009**, *42*, 5861−5872.
(27) Son, J. G.; Gwyther, J.; Chang, J.-B.; Berggren, K. K.; Manners, I.; Ross, C. A. Highly Ordered Square Arrays from a Templated ABC Triblock Terpolymer. *Nano Lett.* **2011**, *11*, 2849−2855.
(28) Xu, Y.; Xie, N.; Li, W.; Qiu, F.; Shi, A.-C. Phase Behaviors and Ordering Dynamics of Diblock Copolymer Self-Assembly Directed by Lateral Hexagonal Confinement. *J. Chem. Phys.* **2012**, *137*, 194905.
(29) He, X.; Song, M.; Liang, H.; Pan, C. Self-Assembly of the Symmetric Diblock Copolymer in a Confined State: Monte Carlo Simulation. *J. Chem. Phys.* **2001**, *114*, 10510−10513.
(30) Yu, B.; Sun, P.; Chen, T.; Jin, Q.; Ding, D.; Li, B.; Shi, A.-C. Confinement-Induced Novel Morphologies of Block Copolymers. *Phys. Rev. Lett.* **2006**, *96*, 138306.
(31) Li, W.; Wickham, R. A. Self-Assembled Morphologies of a Diblock Copolymer Melt Confined in a Cylindrical Nanopore. *Macromolecules* **2006**, *39*, 8492−8498.
(32) Chen, P.; Liang, H.; Shi, A.-C. Origin of Microstructures from Confined Asymmetric Diblock Copolymers. *Macromolecules* **2007**, *40*, 7329−7335.
(33) Miao, B.; Yan, D.; Wickham, R. A.; Shi, A.-C. The Nature of Phase Transitions of Symmetric Diblock Copolymer Melts under Confinement. *Polymer* **2007**, *48*, 4278−4287.
(34) Zhu, Y.; Jiang, W. Self-Assembly of Diblock Copolymer Mixtures in Confined States: A Monte Carlo Study. *Macromolecules* **2007**, *40*, 2872−2881.
(35) Li, S.; Chen, P.; Zhang, L.; Liang, H. Geometric Frustration Phases of Diblock Copolymers in Nanoparticles. *Langmuir* **2011**, *27*, 5081−5089.
(36) Shi, A.-C.; Li, B. Self-Assembly of Diblock Copolymers under Confinement. *Soft Matter* **2013**, *9*, 1398−1413.
(37) Zhang, T.; Deng, H.; Yang, T.; Li, W. Defective Morphologies Kinetically Formed in Diblock Copolymers under the Cylindrical Confinement. *Polymer* **2015**, *65*, 168−174.
(38) Deng, H.; Qiang, Y.; Zhang, T.; Li, W.; Yang, T. Chiral Selection of Single Helix Formed by Diblock Copolymers Confined in Nanopores. *Nanoscale* **2016**, *8*, 15961−15969.
(39) Wu, Y.; Cheng, G.; Katsov, K.; Sides, S. W.; Wang, J.; Tang, J.; Fredrickson, G. H.; Moskovits, M.; Stucky, G. D. Composite Mesostructures by Nano-Confinement. *Nat. Mater.* **2004**, *3*, 816−822.
(40) Xiang, H.; Shin, K.; Kim, T.; Moon, S. I.; McCarthy, T. J.; Russell, T. P. Block Copolymers under Cylindrical Confinement. *Macromolecules* **2004**, *37*, 5660−5664.
(41) Dobriyal, P.; Xiang, H.; Kazuyuki, M.; Chen, J.-T.; Jinnai, H.; Russell, T. P. Cylindrically Confined Diblock Copolymers. *Macromolecules* **2009**, *42*, 9082−9088.
(42) Xu, J.; Russell, T. P.; Ocko, B. M.; Checco, A. Block Copolymer Self-Assembly in Chemically Patterned Squares. *Soft Matter* **2011**, *7*, 3915−3919.
(43) Dessi, R.; Pinna, M.; Zvelindovsky, A. V. Cell Dynamics Simulations of Cylinder-Forming Diblock Copolymers in Thin Films on Topographical and Chemically Patterned Substrates. *Macromolecules* **2013**, *46*, 1923−1931.
(44) Li, W.; Qiu, F.; Yang, Y.; Shi, A.-C. Ordering Dynamics of Directed Self-Assembly of Block Copolymers in Periodic Two-Dimensional Fields. *Macromolecules* **2010**, *43*, 1644−1650.
(45) Li, W.; Xie, N.; Qiu, F.; Yang, Y.; Shi, A.-C. Ordering Kinetics of Block Copolymers Directed by Periodic Two-dimensional Rectangular Fields. *J. Chem. Phys.* **2011**, *134*, 144901.
(46) Xie, N.; Li, W.; Qiu, F.; Shi, A.-C. New Strategy of Nanolithography via Controlled Block Copolymer Self-Assembly. *Soft Matter* **2013**, *9*, 536−542.
(47) Wickham, R. A.; Shi, A.-C.; Wang, Z.-G. Nucleation of Stable Cylinders from a Metastable Lamellar Phase in a Diblock Copolymer Melt. *J. Chem. Phys.* **2003**, *118*, 10293−10305.
(48) Spencer, R. K. W.; Wickham, R. A. Simulation of Nucleation Dynamics at the Cylinder-to-Lamellar Transition in a Diblock Copolymer Melt. *Soft Matter* **2013**, *9*, 3373−3382.
(49) Deng, H.; Xie, N.; Li, W.; Qiu, F.; Shi, A.-C. Perfectly Ordered Patterns via Corner-Induced Heterogeneous Nucleation of Self-Assembling Block Copolymers Confined in Hexagonal Potential Wells. *Macromolecules* **2015**, *48*, 4174−4182.
(50) Ohta, T.; Ito, A. Dynamics of Phase-Separation in Copolymer-Homopolymer Mixtures. *Phys. Rev. E: Stat. Phys., Plasmas, Fluids, Relat. Interdiscip. Top.* **1995**, *52*, 5250−5260.
(51) Ohta, T.; Kawasaki, K. Equilibrium Morphology of Block Copolymer Melts. *Macromolecules* **1986**, *19*, 2621−2632.
(52) Matsen, M. W. New fast SCFT algorithm applied to binary diblock/homopolymer blends. *Macromolecules* **2003**, *36*, 9647.
(53) Joannopoulos, J. D.; Johnson, S. G.; Winn, J. N.; Meade, R. D. *Photonic Crystals: Molding the Flow of Light*; Princeton University Press, 2008.
(54) Song, D.-P.; Li, C.; Li, W.; Watkins, J. J. Block Copolymer Nanocomposites with High Refractive Index Contrast for One-Step Photonics. *ACS Nano* **2016**, *10*, 1216−1223.

DOI: 10.1021/acs.langmuir.6b03638
Langmuir 2016, 32, 13787−13794